Patch-based sparse reconstruction of material BTFs

Dennis den Brok Heinz Christian Steinhausen Matthias Hullin Reinhard Klein
Universität Bonn
Institute of Computer Science II
Friedrich-Ebert-Allee 144
53113 Bonn, Germany
{ denbrok, steinhau, hullin, rk }@cs.uni-bonn.de

ABSTRACT

We propose a simple and efficient method to reconstruct materials' *bidirectional texture functions* (BTFs) from angularly sparse measurements. The key observation is that materials of similar types exhibit both similar surface structure and reflectance properties. We exploit this by manually clustering an existing database of fully measured material BTFs and fitting a linear model to each of the clusters. The models are computed not on per-texel data but on small spatial BTF patches we call *apparent BTFs*. Sparse reconstruction can then be performed by solving a linear least-squares problem without any regularization, using a per-cluster sampling strategy derived from the models. We demonstrate that our method is capable of faithfully reconstructing fully resolved BTFs from sparse measurements for a wide range of materials.

Keywords

bidirectional texture functions, sparse acquisition, material appearance

1 INTRODUCTION

In many applications, it is desirable or even imperative to reproduce a material's appearance faithfully and, possibly, in real-time. For a wide range of materials *bidirectional texture functions* (BTFs) – loosely speaking, an image-based variant of the better known *spatially varying bidirectional reflectance distribution functions* (SVBRDFs) – provide good reproduction quality, even at interactive frame rates. The acquisition of high-quality, high-resolution BTFs of real-world materials is, however, by many means expensive. In particular, measurement times of typically many hours per material make it very cumbersome to obtain large BTF databases, as pictures of the material to be measured have to be taken from many different viewing angles and under many different lighting conditions.

We propose a simple and efficient method for the sparse acquisition of material BTFs, assuming a sufficiently large and heterogenous database of fully measured materials is available:

We demonstrate that linear models describing material reflectance per texel are insufficient for this task because effects not local to texels frequently occur. We show that, instead, small BTF patches we call *apparent BTFs* (ABTFs) provide a suitable foundation for such models. In order to account for the high variance of material surfaces, we propose to fit models to patches clustered by semantic material class. From these models, sparse sampling strategies can be deduced that take advantage of the peculiarities of existing BTF acquisition devices. Reconstruction from such sparse measurements can then be achieved efficiently by solving a simple linear least-squares problem without regularization.

We demonstrate that our method is able to reconstruct fully resolved material BTFs of good quality from as little as 6% of the original samples. It can be used for substantially improving acquisition times or angular resolution, thus benefiting the most common BTF acquisition devices.

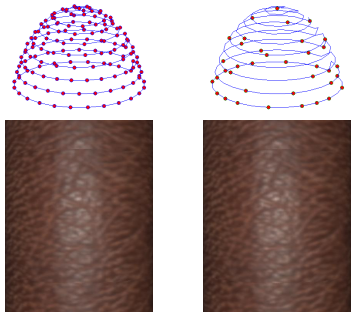

Figure 1: Left: Reference rendering along with the full sampling. Right: Sparse sampling used to produce the rendering of a sparse reconstruction shown below.

2 BACKGROUND

2.1 Bidirectional texture functions

BTFs have been introduced by Dana *et al*. [1] as an image-based approach to spatially varying appearance. Like SVBRDFs, they are 6-dimensional functions of the form

$$\mathscr{B}(\mathbf{x}, \omega_i, \omega_o),$$

where $\omega_{i,o} \in \mathbf{R}^2$ are the incoming and outgoing light directions, respectively, and $\mathbf{x} \in \mathbf{R}^2$ is the position on a parameterized surface V. In the case of material BTFs, V is typically flat; it does not need to coincide with the material's actual surface geometry. It is generally assumed that light sources are directional and have the same spectrum. In particular, effects such as phosphorescene, fluorescence and subsurface scattering cannot be captured accurately.

The fundamental difference from SVBDRFs is that the function $\mathscr{B}(\mathbf{x}, -)$ need not be BRDF-valued: the corresponding per-texel reflectance function does not need to adhere to Helmholtz reciprocity and conservation of energy and is, therefore, capable of capturing non-local effects such as interreflections and self-shadowing. Moreover, because V does not necessarily coincide with the actual surface, the per-texel reflectance functions may also describe parallax effects. For these reasons, the term *apparent BRDF* (ABRDF) has been suggested by Wong *et al*. [18] for this kind of functions. Conversely, the values of the function $\mathscr{B}(-, \omega_i, \omega_o)$ are just 2D textures corresponding to specific pairs of incoming and outgoing light directions.

2.2 BTF acquisition

Several setups for the acquisition of BTFs have been proposed. We briefly review the most prominent paradigms, as our method benefits all of them to a greater or lesser extent. An in-depth overview can be found in [16].

2.2.1 Gonioreflectometer

In what is historically the first BTF acquisition setup, proposed by Dana *et al*. [1], the material sample is placed on a turntable, and a camera and a light source held by robot arms are moved across the hemisphere above the sample to capture images of the sample under different lighting and viewing conditions. The gonioreflectometer is very flexible in terms of possible samplings of the hemisphere, but measurement times are excessive – on the order of weeks for a moderate angular resolution – due to the little amounts of light sources and sensors and the movable parts' low speeds.

2.2.2 Kaleidoscope

Han *et al*. [7] introduced an intriguing parallel setup: The sample is placed underneath a tapered kaleidoscope, lit and captured from a projector and a camera placed at the other end, which allows for a number of lighting and viewing conditions to be measured in a single camera shot. By appropriately arranging the mirrors, the angular and spatial resolution can be adjusted; however, both are typically rather low, and increasing one leads to a decrease of the other, so there is always a tradeoff to be made.

2.2.3 Camera domes

Camera domes as proposed, for instance, by Müller *et al*. [11] and Schwartz *et al*. [15] ideally provide a highly parallel means to acquire BTFs: A number of cameras is spread across the hemisphere above the sample holder. Their flashes or separate LEDs are used as light sources. Parallelism may be traded for fewer cameras and lower cost by placing the sample on a turntable in order to achieve a similarly dense sampling of the hemisphere. Due to the number of cameras, data transfer times become a new bottleneck.

In all of the above setups, it is usually necessary to capture the same scene several times with different shutter times in order to obtain HDR data.

2.3 Related work

To the best of our knowledge, no method for sparse reconstruction of entire BTFs has been proposed so far. There exists, however, a number of methods for lower-dimensional reflectance models:

In [10], Matusik *et al*. perform *singular value decomposition* (SVD) on a database of 100 measured BRDFs of a wide range of isotropic materials to obtain a linear model.

In [9], the same authors introduce two methods for sparse reconstruction of isotropic BRDFs: The first method is based on a wavelet analysis of their BRDF database. A set of basis wavelets termed *common wavelet basis* is determined and used to reconstruct previously unseen BRDFs with approximately 1.5 million samples from approximately 70000 measurements. The second method uses the entire BRDF database itself as a linear model for reconstruction of fully measured BRDFs from as little as 800 out of the original approximately 1.5 million samples, at the cost of slightly increased reconstruction errors and the required availability of the BRDF database. Samples are chosen using a simple optimization algorithm such that the linear system to be solved for reconstruction is well-conditioned. They do not investigate how well their methods generalize to more complex reflectance such as anisotropic BRDFs or ABRDFs.

In [2], Dong *et al*. reconstruct a material's SVBRDF from a sparse measurement using a manifold constructed from analytical BRDFs fit to fully measured BRDFs of manually selected representative points on

the material's surface. The algorithm is unlikely to scale to BTFs because of the typically much higher intrinsic dimensionality of the ABRDF manifold (*cf.* section 4.1.1). A generalization to previously unseen materials is not obvious, albeit conceivable.

Peers *et al.* [13] introduce *compressed sensing* [3] to the acquisition of *reflectance fields*, assuming both 2D *outgoing* (here: fixed viewing direction) and *incident light fields*. Their algorithm uses a hierarchical, multi-resolution Haar wavelet basis, taking spatial coherence into account. It is not clear how to extend this approach to a multi-view setup. Common BTF acquisition setups only have a very limited number of light sources, where the advantage of compressed sensing might be negligible. Due to these light sources' brightness, we expect shot noise to become a problem.

Conversely, in [8], Marwah *et al.* use sparsity-based methods related to compressed sensing in order to sparsely acquire 4D light fields with an angular resolution of 5×5. They compute a dictionary of what they call *light field atoms* – 11×11 spatial light field patches which allow for a sparse representation of natural light fields. Such a dictionary does not exist in the case of ABRDFs or ABTFs; as demonstrated in section 4.1.1, their dimensionality is likely too high.

Filip *et al.* [5] propose a vector quantization of BTFs for the purpose of compression, guided by a psychophysically validated metric. They conclude that as little as 10 – 35 % of the original textures are sufficient to maintain the same visual appearance in renderings. It would be interesting to investigate whether there is a common quantization for *all* materials, and if so, whether it could be used for sparse acquisition. A large user study would be needed in order to adapt the metric to a bigger BTF database.

3 LINEAR MODELS FOR MATERIAL BTFS

During measurement, a finite discretization of the measured material's BTF $\mathscr{B}$ is obtained. After rectification of the acquired images, the discrete BTF has a natural representation as a matrix $\mathbf{B} \in \mathbf{R}^{n \times m}$ with the columns representing the m discrete ABRDFs, each entry corresponding to some pair (ω_i, ω_o) of incoming and outgoing angle, and the rows representing the n rectified textures (*cf.* figure 2).

3.1 Linear models & reconstruction

The goal is now to recover $\mathbf{B}$ from a sparse measurement

$$\widetilde{\mathbf{B}} = \mathbf{M}\mathbf{B}$$

of n_s samples, where $\mathbf{M} \in \mathbf{R}^{n_s \times n}$ is a *measurement matrix*, typically binary, which determines the sparse sampling.

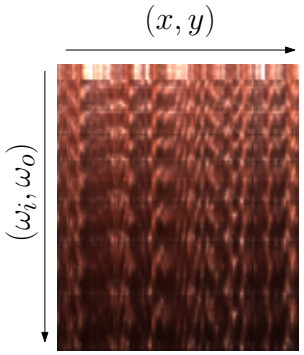

Figure 2: Representation of a discretized BTF as a matrix.

Arguably one of the most simple methods to attack this problem is, given fully resolved training data $\mathbf{D}$, to fit a linear model $\mathbf{D} \approx \mathbf{UC}$. An optimal fitting method in terms of L^2 error is to compute a truncated SVD

$$\mathbf{D} \approx \mathbf{U}\Sigma\mathbf{V}^t$$

as established by the Eckart-Young theorem [4]. The hope is that the model both

- generalizes to previously unknown data; *i.e.*

$$\min_{\mathbf{C_B}} \|\mathbf{UC_B} - \mathbf{B}\| < \varepsilon \tag{1}$$

- is expressive enough that a sparse sampling is sufficient to find reasonable coefficients; *i.e.*

$$\min_{\mathbf{C_B}} \|\mathbf{M}(\mathbf{UC_B} - \mathbf{B})\| < \delta \implies \|\mathbf{UC_B} - \mathbf{B}\| < \varepsilon \tag{2}$$

Provided $\widetilde{\mathbf{B}}$ has at least as many rows as columns, an approximation of $\mathbf{B}$ may then be obtained via

$$\mathbf{B} \approx \mathbf{U}(\mathbf{MU})^{\dagger}\widetilde{\mathbf{B}}, \tag{3}$$

where $(\mathbf{MU})^{\dagger}$ denotes the Moore-Penrose pseudo-inverse of $\mathbf{MU}$.

It is well-known that the fitting of linear models through minimization of L^2 error is sensitive to outliers. In order to decrease the influence of specular highlights, we reduce the data's dynamic range by converting the measured HDR RGB data to YUV color space, dividing the U and V values by the corresponding Y value and applying log to the Y values.

Despite its simplicity, this approach has been demonstrated in [9] to be quite effective in the special case of isotropic BRDFs. It seems thus worthwhile to investigate whether this generalizes to ABRDFs.

3.2 Linear models for ABRDFs

Linear models for ABRDFs are already being used for compression and rendering of BTFs, often under the

moniker *full matrix factorization* (FMF). In that case, models are fit to a certain material's ABRDFs only; *i.e.* to $\mathbf{B}$ instead of a whole database $\mathbf{D}$. The columns of $\mathbf{U}$ and $\mathbf{V}$ are commonly refered to as *eigen-ABRDFs* and *eigentextures*, respectively [12], in reference to their semantic meaning.

It is reasonable to assume that for BTFs the ABRDFs of which are close to being true BRDFs, a linear model may perform similarly well as in [9] [10] with respect to equations 1 and 2. However, as soon as surface structure becomes significant, reconstructions from sparse measurements might easily miss effects such as self-shadowing, interreflections, occlusion and parallax. We shall demonstrate in section 4.2 that this is indeed the case.

3.3 Linear models for ABTFs

In order to overcome these problems, we take spatial information into account: instead of considering only ABRDFs, we consider entire collections of neighboring ABRDFs, which we call *apparent BTFs* (ABTFs), as similar to ABRDFs they capture effects not local to the specific patch such as interreflections or shadows cast from neighboring patches.

The matrix $\mathbf{B}$ then takes on a different form, with its columns representing discrete ABTFs, for instance as vectors of stacked discrete ABRDFs belonging to the same neighborhood. The corresponding measurement matrix becomes $\mathbf{1}_{p^2} \otimes \mathbf{M}$, where p denotes the spatial patch size and $\otimes$ the Kronecker product.

Note that an alternative to patches exists in the form of appropriate filter banks, as *e.g.* demonstrated by Peers *et al.* [13] A case has been made in favor of the simpler spatial patches by Varma *et al.* [17], albeit in the case of material classification: the authors demonstrate that classification using spatial patches, which can be as small as 3×3 texels, is superior to that using filter banks with equivalent support.

The intrinsic dimensionality of the ABTF database is likely higher than that of the ABRDF database; in the worst case by a factor equal to the patch size. To mitigate this to some extent, we propose to cluster the database such that each cluster contains only materials with similar surface structure, and determine the linear models $\mathbf{D}_{\text{cluster}} \approx \mathbf{U}\Sigma\mathbf{V}^t$ per cluster. The columns of $\mathbf{U}$ shall be called *eigen-ABTFs*.

3.4 Sampling strategies

Once a model satisfying equation 1 has been established, a measurement matrix $\mathbf{M}$ that takes advantage of the model needs to be devised. We chose to implement the simple optimization algorithm proposed in [10]:

$\mathbf{M} \in \mathbf{R}^{n_s \times n}$ is initialized as random binary matrix with precisely one 1 on each row. The algorithm then randomly replaces one row of $\mathbf{M}$ with a different random binary unit row vector. If the condition number $\kappa(\mathbf{MU})$ does not decrease, the change is reverted. This is repeated until convergence or a maximum number of steps is reached (*cf.* algorithm 1). For ABTFs, the condition number $\kappa((\mathbf{1}_{p^2} \otimes \mathbf{M})\mathbf{U})$ is tested instead.

The intuition behind this choice is that the condition number $\kappa(\mathbf{MU})$ is an indicator of how robustly $\mathbf{MU}$ can be inverted; *i.e.* of how well coefficients $\mathbf{C_B}$ as in equation 2 can be found.

In its present form the algorithm is free to choose whatever pairs of incoming and outgoing light directions lead to well-conditioned linear system. This approach suits best the gonioreflectometer setup, where all such pairs have equal costs. The algorithm can easily be modified to take the parallelism of camera dome setups into account.

While undersampling could be used in the kaleidoscope setup as well, we argue it is more beneficial to use the proposed method in order to increase the kaleidoscope's limited angular resolution.

Algorithm 1 Generation of a measurement matrix.

Input: desired number n_s of samples
Output: optimized measurement matrix $\mathbf{M} \in \mathbf{R}^{n_s \times n}$
  $\mathbf{M} \leftarrow$ random binary with exactly one 1 per row
  while not converged **do**
    $\mathbf{M}' \leftarrow \mathbf{M}$
    $\mathbf{r} \leftarrow$ random binary row vector with $\|\mathbf{r}\|_0 = 1$
    random row of $M \leftarrow \mathbf{r}$
    if $\kappa(\mathbf{M}'\mathbf{U}) < \kappa(\mathbf{MU})$ **then**
      $\mathbf{M} \leftarrow \mathbf{M}'$
    end if
  end while
  return $\mathbf{M}$

4 RESULTS

For our experiments, we used an existing database of high-quality measured BTFs. The measurement device used to create the database is a camera dome with 151 cameras, the flashes of which are used as light sources, resulting in an angular resolution of 151×151 (*cf.* figure 3a). The rectified textures have a spatial resolution of 512×512 pixels and correspond to a part of the sample approximately $4\text{ cm} \times 4\text{ cm}$ in size. The database consists of 14 semantic classes with 12 materials each. We selected the classes *carpet*, *cloth*, *gravel*, *leather*, *metal*, *stone*, *wall tile*, *wallpaper* and *wood*, which exhibit significant inter- and intraclass variance. We used 11 materials per class for fitting the linear models and the remaining material per class for the purpose of validation.

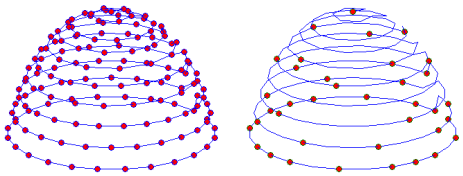

(a) (b)

Figure 3: (a) Sketch of the acquisition setup. The red points correspond to both light sources and cameras. (b) Sketch of the 7 × 7 parabolic map sampling. The red points correspond to both light sources and cameras.

All computations have been performed using MATLAB 2011b under Windows XP on a machine with two Intel Xeon E5645 processors and 144 GB of RAM.

4.1 Model fitting

Computing at once a truncated SVD for either of the entire database, or even single clusters thereof, is prohibitive due to the computation time required. We therefore used *eigenspace merging* to compute the SVD hierarchically; *i.e.* we first use EM-PCA (*cf.* [14]) to obtain approximate truncated SVDs of the single BTFs and subsequently merge the resulting eigenspaces (*cf. e.g.* [6]). In order to further reduce computation times, we cropped the BTFs to a spatial extent of 128×128 texels. For the purpose of comparison, we fit linear models both to the ABRDF and the ABTF database.

4.1.1 ABRDFs

For a single one of our BTFs, 200 eigen-ABRDFs for the $\log(Y)$ channel and 100 eigen-ABRDFs for each the U/Y and the V/Y channel provide a very high reproduction quality. We merged the resulting eigenspaces first per cluster and then globally to obtain an ABRDF basis of 2048 eigen-ABRDFs. The entire process takes approximately 30 minutes per cluster, including disk I/O and the color space transformation, hence about 4.5 hours altogether.

Table 1 shows the relative projection errors ε that occur when projecting the $\log(Y)$ channel of the test material's BTF onto the corresponding bases for various numbers of basis ABRDFs; *i.e.*

$$\varepsilon = \frac{\|\mathbf{U}(\mathbf{U}'\mathbf{B}) - \mathbf{B}\|_{\mathrm{F}}}{\|\mathbf{B}\|_{\mathrm{F}}}$$

where $\|\cdot\|_{\mathrm{F}}$ denotes the Frobenius norm. For comparison, we include the relative projection errors for the fully measured BTFs after FMF-compression retaining 128 eigen-ABRDFs, a number suitable for high-quality real-time rendering. Typically, 1024 basis ABRDFs are sufficient to achieve good projection results, which is the lower limit on the number of samples necessary for sparse reconstruction via equation 3.

4.1.2 ABTFs

For ABTFs, we computed bases per cluster. Following the argument in [17], we used a spatial ABTF size of 3×3. For performance reasons, we selected ABTFs maximally without overlap, resulting in a database of 1764 ABTFs per material and 19404 ABTFs per cluster. We again first computed bases per-material, retaining 200 eigen-ABTFs for the $\log(Y)$ channel and 100 eigen-ABTFs for each the U/Y and the V/Y channel, and then merged the resulting eigenspaces per cluster. This process takes approximately 2 hours per cluster, or 18 hours in total.

Table 1 shows relative projection errors (*cf.* section 4.1.1) for the $\log(Y)$ channel for 1024 and 2048 basis ABTFs in comparison with errors for reconstructions from ABRDF-wise projections. The projections themselves were produced by collecting all possible 3 × 3 ABTFs from the test BTF and projecting them onto the appropriate cluster's basis. BTFs are obtained from this representation by computing the reconstruction and blending the patches, all texels weighted equally. Typically, 2048 basis ABTFs provide almost as good projections results as 1024 basis ABRDFs.

4.2 Reconstruction

Figure 4 shows renderings of BTFs reconstructed with the proposed method, table 2 the corresponding relative reconstruction errors

$$\varepsilon = \frac{\|\mathbf{U}((\mathbf{M}\mathbf{U})^{\dagger}\widetilde{\mathbf{B}}) - \mathbf{B}\|_{\mathrm{F}}}{\|\mathbf{B}\|_{\mathrm{F}}}.$$

For comparison, we include renderings of the FMF-compressed original fully measured BTFs and their sparse reconstructions from ABRDF-wise linear models, along with the relative projection errors, which constitute lower limits for the relative reconstruction errors. BTFs were produced from ABTF-wise sparse reconstructions as described in section 4.1.2. We used two different sampling strategies: a 7 × 7 parabolic map mapped to the closest light and camera positions of the acquisition setup's full sampling, which may be considered a vague approximation of a kaleidoscope's sampling (*cf.* figure 3b), and optimized samplings with the same number of samples produced by algorithm 1. Both samplings consist of 1369 samples in total, or 6 % of the original 22801 samples.

4.2.1 ABRDFs

As predicted in section 3.2, ABRDF-wise reconstruction produces acceptable results only for materials with simple surface structure and reflectance – here: *stone* and *wood* – and even then only with the optimized sampling. *Leather* and *metal* already exhibit annoying artifacts; the results for even more complex materials are unsuitable for any practical purpose.

		# basis ABRDFs					# basis ABTFs	
class	FMF	128	256	512	1024	2048	1024	2048
carpet	5.4	6.2	5.6	5.1	4.6	4.0	5.3	5.1
cloth	2.7	4.0	3.2	2.6	2.1	1.7	2.9	2.7
gravel	5.0	8.0	6.7	5.6	4.7	4.0	5.4	4.9
leather	1.5	2.9	2.4	2.0	1.6	1.3	1.9	1.8
metal	1.0	3.2	2.5	2.1	1.8	1.6	2.7	2.2
stone	0.6	3.1	2.5	2.0	1.5	1.2	1.8	1.5
wall tile	0.4	5.6	4.7	3.8	2.9	2.1	2.2	1.7
wallpaper	2.7	5.2	4.4	3.6	3.0	2.4	3.4	3.1
wood	0.8	2.3	1.9	1.6	1.3	1.0	1.2	1.1

Table 1: $\log(Y)$ channel relative L^2 projection errors in percent for various numbers of basis ABRDFs. FMF: Projection onto per-material ABRDF basis with 128 eigen-ABRDFs.

	ABRDF			ABTF		
class	proj	pmap7	optimized	proj	pmap7	optimized
carpet	4.6	27.6	11.4	5.1	7.3	6.3
cloth	2.1	11.1	5.4	2.7	3.6	3.2
gravel	4.7	26.7	11.8	4.9	8.0	7.0
leather	1.6	8.0	4.0	1.8	2.3	2.1
metal	1.8	8.8	4.6	2.2	3.8	3.3
stone	1.5	6.3	3.4	1.5	2.3	2.3
wall tile	2.9	10.0	6.3	1.7	6.9	6.8
wallpaper	3.0	14.8	7.0	3.1	4.2	4.2
wood	1.3	6.3	2.9	1.1	1.6	1.5

Table 2: $\log(Y)$ channel relative L^2 reconstruction errors per cluster in percent. proj: Projection onto common basis. pmap7: Results for reconstruction from parabolic map sampling. optimized: Results for reconstruction from optimized sampling.

4.2.2 ABTFs

In contrast, even the non-optimized sampling is sufficient to produce convincing reconstructions of moderately complex materials using ABTF models. Where it is not, the optimized sampling often helps; only *gravel* and *wallpaper* exhibit perceivable artificats. The highlight of *wall tile* is not quite as sharp as it should be, and there are some artifacts in the highlight of *metal* visible mostly in the corresponding amplified error image (*cf.* figure 4f).

4.3 Limitations

While the proposed algorithm performs well in many situations, it has a number of limitations:

Most notably, it relies on the availability of a database of fully measured BTFs. Depending on the materials to be measured, that database must be quite encompassing; however, if *e.g.* only leathers are going to be measured, then a small database of a few measured leather BTFs might already be sufficient.

Without any regularization the lowest possible number of samples is precisely the number of basis ABTFs divided by the patch size. Typically, a greater number is necessary for robust results.

Reconstructions of material BTFs with highly complex surface structure may still suffer from artifacts visible in common lighting scenarios. It is not clear whether larger patch sizes could mitigate this. Even if so, this would likely lead to an undesirable significant increase of computation times and memory consumption.

For the same reason, the algorithm is constrained to moderate sampling rates. It would also be difficult to bootstrap a sufficiently large and heterogenous BTF database with substantially higher sampling rates.

5 CONCLUSION

We demonstrated the general possibility of efficient sparse acquisition of BTFs for a wide range of materials, provided a database of fully measured optically similar materials is available.

It would be interesting to investigate whether our results could be improved further. A possible approach is to further improve the linear bases, for instance by feature-aligning the ABTFs prior to fitting the models. It is also unclear how suitable our manual clustering of the database actually is. Automatic methods might be able to find a better optimization, possibly even consisting of fewer classes.

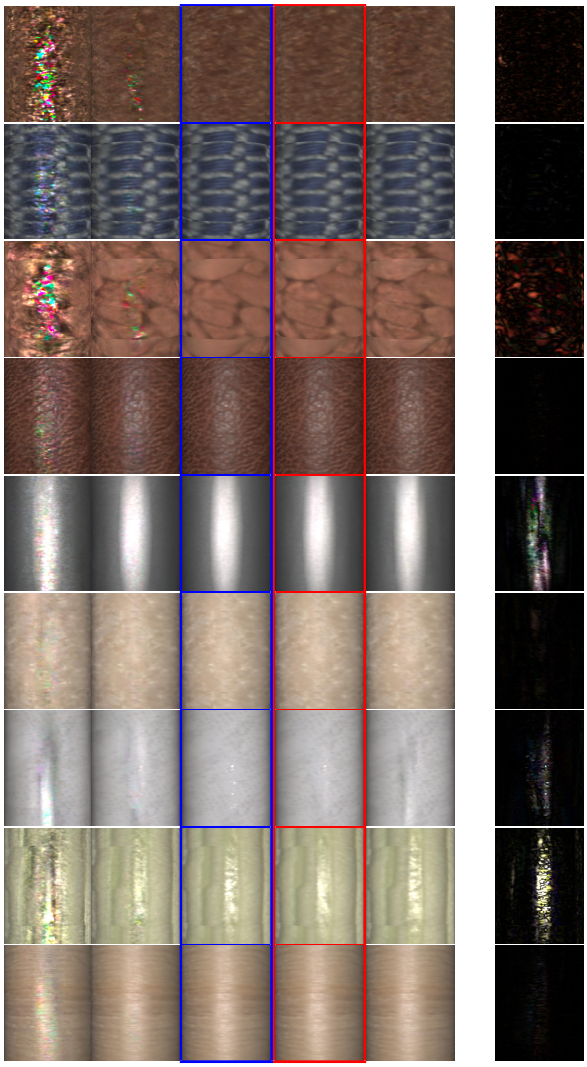

(a) (b) (c) (d) (e) (f)

Figure 4: Renderings of reconstruction results.
(a) ABRDF-based reconstructions from 7 × 7 parabolic map sampling (1369 samples).
(b) ABRDF-based reconstructions from optimized sampling (1369 samples).
(c) FMF-compressed ground truth (22801 samples).
(d) ABTF-based reconstructions from optimized sampling (1369 samples).
(e) ABTF-based reconstructions from 7 × 7 parabolic map sampling (1369 samples).
(f) 20 × absolute differences between (c) and (d).

Moreover, our linear models might also be useful for purposes other than sparse reconstruction; for instance, it might be possible to use them to leverage the quality of BTF measurements produced with consumer-grade hardware, or under conditions less controlled than in the discussed setups.

Although the improvement in measurement cost is significant, the amount of samples needed still leaves room for further improvement. Depending on the material, it should not be impossible — at least given a rough estimate of the material's surface structure — to obtain satisfactory reconstruction results from less than 100 images. Both our experiments and compressed sensing theory suggest, however, that this barrier cannot be broken merely using unregularized linear methods. It thus seems worthwhile to investigate non-linear methods such as manifold learning or texture synthesis.

6 ACKNOWLEDGEMENTS

This work was funded by the X-Rite graduate school on Digital Material Appearance.

7 REFERENCES

[1] Kristin J. Dana, Bram van Ginneken, Shree K. Nayar, and Jan J. Koenderink. Reflectance and texture of real-world surfaces. *ACM Trans. Graph.*, 18(1):1–34, January 1999.

[2] Yue Dong, Jiaping Wang, Xin Tong, John Snyder, Yanxiang Lan, Moshe Ben-Ezra, and Baining Guo. Manifold bootstrapping for SVBRDF capture. *ACM Trans. Graph.*, 29(4):98:1–98:10, July 2010.

[3] David L. Donoho. Compressed sensing. *IEEE Trans. Inform. Theory*, 52:1289–1306, 2006.

[4] Carl Eckart and Gale Young. The approximation of one matrix by another of lower rank. *Psychometrika*, 1(3):211–218, 1936.

[5] Jiří Filip, Michael J. Chantler, Patrick R. Green, and Michal Haindl. A psychophysically validated metric for bidirectional texture data reduction. *ACM Trans. Graph.*, 27(5):138:1–138:11, December 2008.

[6] Peter Hall, David Marshall, and Ralph Martin. Merging and splitting eigenspace models. *IEEE Trans. Pattern Anal. Mach. Intell.*, 22(9):1042–1049, September 2000.

[7] Jefferson Y. Han and Ken Perlin. Measuring bidirectional texture reflectance with a kaleidoscope. *ACM Trans. Graph.*, 22(3):741–748, July 2003.

[8] Kshitij Marwah, Gordon Wetzstein, Yosuke Bando, and Ramesh Raskar. Compressive light field photography using overcomplete dictionaries and optimized projections. *ACM Trans. Graph.*, 32(4):46:1–46:12, July 2013.

[9] Wojciech Matusik, Hanspeter Pfister, Matt Brand, and Leonard McMillan. A data-driven reflectance model. *ACM Trans. Graph.*, 22(3):759–769, July 2003.

[10] Wojciech Matusik, Hanspeter Pfister, Matthew Brand, and Leonard McMillan. Efficient isotropic BRDF measurement. In *Proceedings of the 14th Eurographics Workshop on Rendering*, EGRW

'03, pages 241–247, Aire-la-Ville, Switzerland, Switzerland, 2003. Eurographics Association.

[11] Gero Müller, Gerhard H. Bendels, and Reinhard Klein. Rapid synchronous acquisition of geometry and BTF for cultural heritage artefacts. In *The 6th International Symposium on Virtual Reality, Archaeology and Cultural Heritage (VAST)*, pages 13–20. Eurographics Association, Eurographics Association, November 2005.

[12] Gero Müller, Jan Meseth, and Reinhard Klein. Compression and real-time rendering of measured BTFs using local PCA. In *Vision, Modeling and Visualisation 2003*, pages 271–280. Akademische Verlagsgesellschaft Aka GmbH, Berlin, November 2003.

[13] Pieter Peers, Dhruv K. Mahajan, Bruce Lamond, Abhijeet Ghosh, Wojciech Matusik, Ravi Ramamoorthi, and Paul Debevec. Compressive light transport sensing. *ACM Trans. Graph.*, 28(1):3:1–3:18, February 2009.

[14] Sam Roweis. EM algorithms for PCA and SPCA. In *Proceedings of the 1997 Conference on Advances in Neural Information Processing Systems 10*, NIPS '97, pages 626–632, Cambridge, MA, USA, 1998. MIT Press.

[15] Christopher Schwartz, Ralf Sarlette, Michael Weinmann, and Reinhard Klein. DOME II: A parallelized BTF acquisition system. In *Eurographics Workshop on Material Appearance Modeling: Issues and Acquisition*, pages 25–31. Eurographics Association, June 2013.

[16] Christopher Schwartz, Ralf Sarlette, Michael Weinmann, Martin Rump, and Reinhard Klein. Design and implementation of practical bidirectional texture function measurement devices focusing on the developments at the university of bonn. *Sensors*, 14(5), April 2014.

[17] Manik Varma and Andrew Zisserman. A statistical approach to material classification using image patch exemplars. *IEEE Trans. Pattern Anal. Mach. Intell.*, 31(11):2032–2047, November 2009.

[18] Tien-Tsin Wong, Pheng-Ann Heng, Siu-Hang Or, and Wai-Yin Ng. Image-based rendering with controllable illumination. In *Proceedings of the Eurographics Workshop on Rendering Techniques '97*, pages 13–22, London, UK, UK, 1997. Springer-Verlag.